A Fast and Accurate Thermistor String*

H. VAN HAREN, R. GROENEWEGEN, M. LAAN, AND B. KOSTER

Netherlands Institute for Sea Research, Den Burg, Netherlands

(Manuscript received 21 May 1999, in final form 17 April 2000)

ABSTRACT

A ''fast thermistor string'' has been built to accommodate the scientific need to accurately monitor internal wave activity in shelf seas and above sloping bottoms in the ocean. The performance of the thermistors and their custom-designed electronics allow temperature variations to be registered at an estimated relative accuracy better than 0.5 mK with a response time faster than 0.25 s. Quantization noise is less than about 40 μK and dominates instrumental noise. Currently, the string holds 32 sensors, which are sampled within 4 s. When sampling every 30 s, the batteries and the memory capacity of the recorder allow deployments up to 3 months. In all respects, this performance is about an order of magnitude superior to thermistor strings currently available commercially. Moored in combination with an acoustic Doppler current profiler the thermistor string provides data to estimate directly quasi-turbulent (high-frequency internal wave band) vertical temperature fluxes and flux gradients. Examples of field observations are given, which show enhanced levels of temperature variance extending above the canonical internal wave spectral levels near the buoyancy frequency, and detailed variations of high-frequency internal wave variability.

1. Introduction

Waves are abundant in the density stratified interior of the ocean and such ''internal waves'' are thought to be the key to processes involving mixing of momentum and mass, especially above sloping sides of ocean basins (Armi 1978; Munk 1981; Eriksen 1985; Thorpe 1987). In essence, they are the bridge between the large-scale motions in the ocean, which vary in time at tidal periods or longer, and the small turbulence motions down to centimeter spatial scales and 0.01 s timescales, at which motions irreversibly dissipate to heat. However, not all details of the internal wave motions have yet been revealed from field studies, and sources and sinks have not been properly established, so that a revived interest in the subject has been observed.

Internal waves can be monitored by measuring the variations in time of the temperature distribution [as a measure for density (ρ) variations] and its vertical gradient, or by measuring current velocities. The frequency (σ) of internal waves is limited to $f < \sigma < N$, where, at the high end, $N = [-g(d\ln\rho/dz)]^{1/2}$, the buoyancy frequency, with g the acceleration of gravity, pointing in the downward, negative z direction. At the low end, the local inertial frequency is given by $f = 2\Omega\sin\varphi$, and related to the normal component (measured at a latitude φ) of the earth's angular momentum vector $\mathbf{\Omega}$.

Vertical length scales are dictated by the density stratification and the local water depth, and typically range from 1 m near river outflows to several hundreds of meters in the open ocean. Most of the internal wave energy is contained in the larger-scale motions, so that the spectral distribution is red, and energy decays at a (canonical) rate of σ^{-2} in frequency (Garrett and Munk 1979). Internal waves appear not only as linear waves, and, in the time domain, nonlinear internal waves show steep ramps, that is, sudden temperature changes within a few seconds only (Thorpe et al. 1990).

Nonlinear internal waves may be important for the (re)distribution of momentum and mass by means of (vertical) mixing. They result from linear waves interacting with themselves (e.g., Mihaly et al. 1998), or with (noninternal wave) variations in the flow (van Haren et al. 1999), or bottom topography. When internal wave energy is enhanced locally, which should be observable from departures from the canonical internal wave spectrum, the vertical gradients of horizontal currents (shear) will be enhanced too, so that small, high-frequency waves become deformed and eventually break (Eriksen 1985; Thorpe 1987; Gilbert 1993; Eriksen 1998).

As a result, observational studies require measurements of temperature variations in space and time to

* Netherlands Institute for Sea Research Contribution Number 3368.

Corresponding author address: Dr. Hans van Haren, Netherlands Institute for Sea Research, P.O. Box 59, 1790 AB Den Burg, Netherlands.
E-mail: hansvh@nioz.nl

TABLE 1. Specifications of the NIOZ fast thermistor string (NFTS v.1.0).

Characteristic	Specification
No. of sensors	32 (at 1.0-m intervals)
Max no. of sensors	128
Depth rating	6000 m
Range (T)	−5 to 55°C
Accuracy	<0.5 mK
Resolution	≅30–50 μK
Thermistors (two per sensor)	Siemens Matsushita B57017-K822
Self-heating	≅300 μK
Response time (τ)	<0.25 s (in water)
Total sampling time	<4 s (for 32 sensors)
Minimal sampling interval (Δt)	20 s (dependent on disk access)
Memory and battery life	100 days (Δt = 30 s; 32 sensors)

better resolve the buoyancy period and preferably in conjunction with measurements of variations of all three current components. In the latter case, the relative importance of (vertical) fluxes of high-frequency internal wave band fluctuations can be studied, under the assumption of the appropriateness of a Reynolds decomposition of each measured quantity in a low- and high-frequency portion (van Haren et al. 1994).

In order to accommodate this scientific interest the NIOZ fast thermistor string (NFTS) has been developed and built at the Netherlands Institute for Sea Research (in Dutch abbreviated as NIOZ), because no commercially available instrument on the market meets all the requirements. A standard Aanderaa thermistor string holds 11 thermistors, which have an accuracy of 0.1°C and a time constant of more than 1 min, and its recorder can hold a maximum of 15 days of data, when sampling 1 $(\text{min})^{-1}$. Our specific aim is to have a thermistor string that resolves the finest (nonlinear) internal wave fluctuations and scales and that can be moored in combination with an acoustic Doppler current profiler (ADCP), which measures vertical profiles of all three components of current velocity. This requires temperature sensors that are better than 1 mK in accuracy, having a response time of less than 1 s, with a sampling rate faster than 1 $(\text{min})^{-1}$ for a period of 3–4 weeks while the instrument is deployed at depths of typically 1000 m.

2. Instrumentation

a. Technical aspects

The required thermistor is chosen considering that it be robust, pressure resistant (>600 bar), fully sealable, reasonably fast (response time $\tau < 1$ s), and stable.

The scientific requirements are met (Table 1) by using a matched pair of thermistors, which are the frequency determining components of a Wien bridge oscillator. By counting a very high frequency (8 MHz) during exactly 128 periods of the Wien bridge oscillator, a sufficiently high resolution, corresponding to about 40 μK, is obtained. The sampling time of one thermistor is less than 0.1 s. An impulse response time of about 0.25 s in water has been determined, which is sufficient to adequately sample the finest (breaking) internal wave timescales. It may be calculated that self-heating is less than 300 μK, and this remains a constant value. Diagnostic measurements show that the noise present in the digital signal comes predominantly from quantification (section 3a).

The glass-embedded thermistors plus electronics board are held inside a pressure resistant steel protection cage (Fig. 1). As a result, the thermistors do not suffer from pressure hysteresis. A five-pole pressure feedthrough connects the electronics board to a breakout in the main umbilical. The stainless steel parts forming the pressure housing are not screwed or bolted together, but held in position by use of a rubber boot (3M PST). To date, this sensor setup has failed only once, as a single thermistor broke in six deployments at sea.

The data are centrally logged on a hard disk after sequentially addressing and reading the separate electronics boards connected to each set of thermistors (temperature modules). Each module has its own specific address allowing easy exchange. Physical replacement of each thermistor is also easy to accomplish as they are attached to the main umbilical using the rubber boot, which only needs to be peeled off for access. The entire sampling of the thermistor string is completed within 4 s, so that a vertical profile is sampled about 10 times faster than by a standard CTD. However, the current minimum rate of storing samples is 20 s, because the hard disk occasionally requires up to 10 s to write a data block, consisting of several hundreds of profiles.

The central stress member in the main cable is a 1000-kg safe working load 5-mm steel cable, so that the thermistor string can be moored in line. The main electronics, the power supply, and the hard disk are contained in a Benthos spherical glass instrument housing, so that the entire instrumentation is about neutrally buoyant in water. The endurance of batteries and the capacity of the hard disk allow the NFTS to be operationally stand-alone for periods up to three months, depending on the sampling frequency and number of sensors mounted (Table 1).

The thermistor string can support 128 sensors. Its first version has been fitted with 32 sensors at a fixed 1-m spacing as it has been designed for boundary layer studies above sloping sides of ocean basins and for studies in stratified shelf seas. Currently, the sensors are molded into a fixed-length string, so that data can be logged into a central storage unit. However, the thermistor string can be used in a semi-flexible fashion by folding it and attaching it to an additional stress member, so that finer (vertical) scales can be resolved, for example in shallow seas and bays.

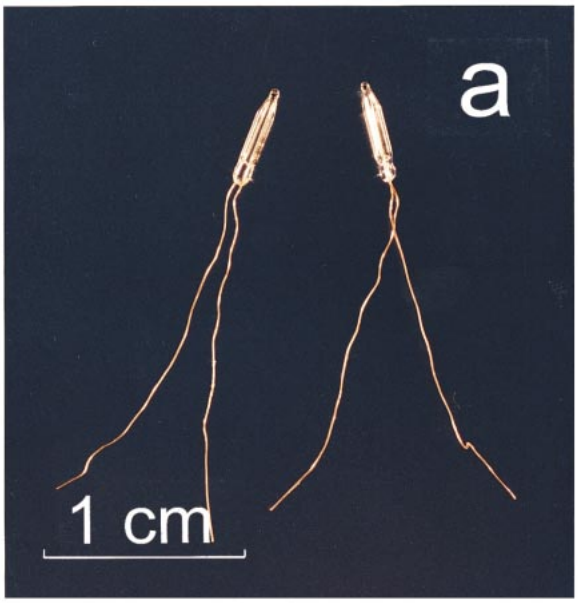
a
1 cm

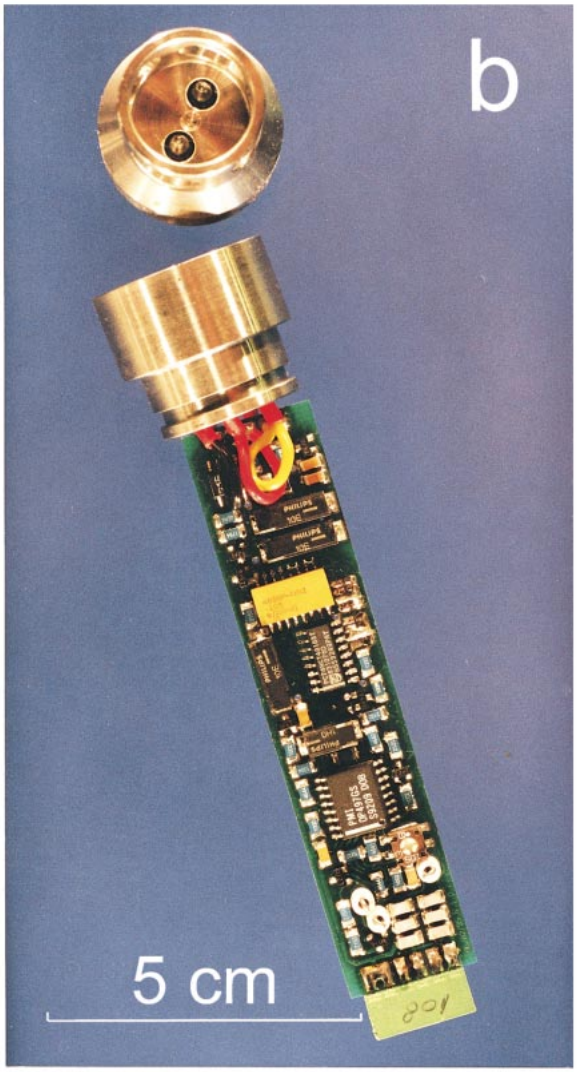
b
5 cm


c
5 cm

b. Calibration

Calibration down to the quantization or self-heating noise levels is beyond our reach. A ''best achievable'' calibration has been performed, which is a time consuming and complicated activity. The NFTS has been calibrated at our institute. A reference thermometer and (maximum) four thermistors are brought together tip-to-tip in a throughflow pipe inside a 2 m^3 stabilized tank. For each group of four thermistors and for one temperature calibration the bath takes about 1 day to become stable to within a few millikelvins, which sets the minimum possible accuracy.

The resulting calibration is better than 3 mK, while being referenced to the triple point of water. Attempts have been made to calibrate the thermistor string in the ocean, by having it curled up and attached to the frame of a Seabird-911 CTD, and by having it curled up and tied to an anchored ship in a highly energetic (tidal currents >1 m s^{-1}) and ''well mixed'' environment. In the latter case, several CTD casts were taken for calibration purposes. In general, these ''calibrations'' are not better than the laboratory calibration, due to the environmental variability, mooring frame vibrations, and flow obstructions. They do provide information about the performance of the NFTS and of the environmental variability that can be resolved. The question of whether a suitable ocean environment for calibration purposes can be found remains unresolved and even if it can be found it may not be easily accessible.

c. Recommended additional data

CTD measurements have not only been used for calibrating the thermistor string. They are also necessary in any study on internal waves in providing information on density dynamics. Following the equation of state, the largest contributions to density variations are not only from temperature variations, but also from salinity and, to a lesser extent, pressure. To address this shortfall of the NFTS, a reasonable number of CTD casts near the location and parallel to the measurements of the NFTS provide insight to the relative contributions to density variations by monitoring the temperature–salinity (*T–S*) relationship, which is often tight.

When this *T–S* relationship is not tight during the mooring period, problems arise in determining the ''background'' buoyancy frequency, and the NFTS data are restricted to an analysis in terms of variations of the temperature field only, albeit this provides sufficient useful information. Especially when the NFTS is moored in conjunction with an ADCP, measuring the vertical velocity component and covering the same range of depths, contributions to vertical fluxes of heat can be studied on contributions to vertical mixing (van Haren et al. 1994; Gemmrich and van Haren 2000 manuscript submitted to *J. Mar. Res.*, hereafter GV). Such a mooring configuration may also provide information on the variability of the water column stability by relating vertical temperature gradients and shear; although in this case, as before, the *T–S* relationship should be known. Further indications for vertical mixing are inferred from the distribution and evolution of isopycnal separation and straining (Pinkel et al. 1991) and from temperature (density) inversions (Thorpe 1987).

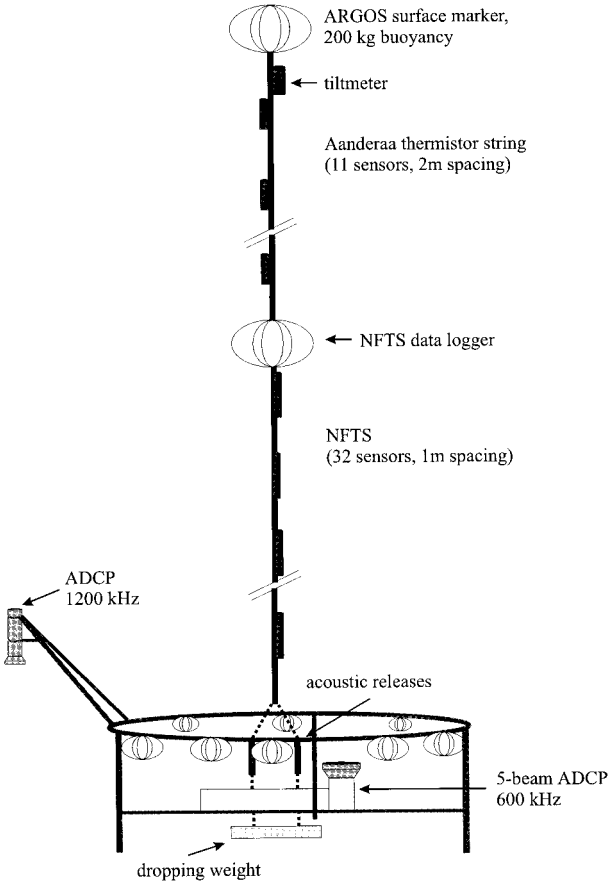

FIG. 2. Mooring configuration.

d. The mooring configuration

The NFTS is usually moored in conjunction with ADCP's mounted in a NIOZ bottom-landing frame (Fig. 2). Currently, this bottom lander holds an upward-looking 600-kHz five-beam RDI-broadband ADCP inside a

←

FIG. 1. Core of the NFTS. (a) The glass-embedded thermistors are held inside (b) a steel protection cage, which is connected to its matching small technology electronics board. (c) The stainless steel pressure housing covering the electronics inside the rubber boot, with the lead to the main umbilical.

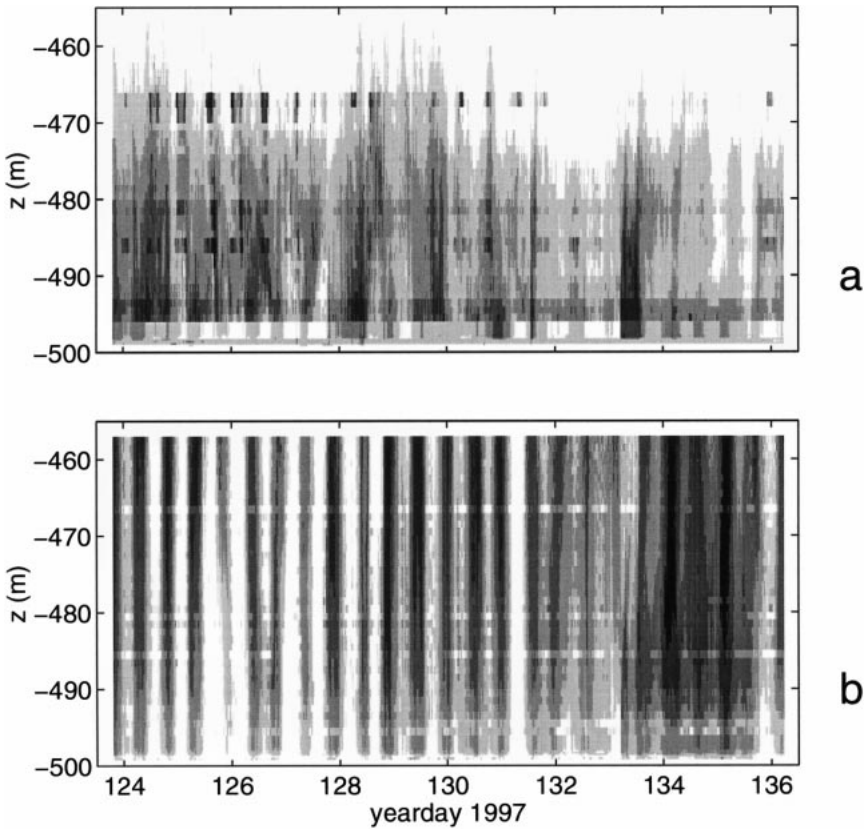

FIG. 3. Contamination of ADCP data by the NFTS varying with tidal periods when moored as in Fig. 2 at a depth of 500 m above the sloping sides of a continental shelf. (a) Raw back-scattered echo intensity [scale varies linearly between 40 (white) and 140 dB (black)]. These data are contaminated due to ensonification of the NFTS data recorder at 466-m depth and the NFTS (sensors) at three depths closer to the bottom. (b) Uncorrected current amplitude (scale varies linearly from white to black between 0 and 50 cm s^{-1}), showing bias toward lower values at depths corresponding to where echo intensity is enhanced due to occasional ensonification of the NFTS.

3.2-m circle of Benthos glass spheres for buoyancy. A downward-looking 1200-kHz RDI-broadband ADCP is mounted 3.2 m above the bottom, so that the beams are pointing away from the frame to guarantee an unobstructed ''view.''

With these ADCPs, the full 3D water velocity is measured at 0.25–0.5-m intervals (bins) over a range of about 50 m, starting at 0.3 m above the bottom. The mooring is recovered using two Benthos acoustic releases mounted in the frame, which uncouple the NFTS and the main 500-kg dropping weight from the bottom frame simultaneously, so that the thermistor string and the bottom lander surface separately. Currently, a second, modified Aanderaa thermistor string holding 11 sensors at 2-m intervals is mounted above or below the NFTS to cover fully the range of the upward-looking ADCP, albeit at a lesser performance. Above the thermistor strings a tilt meter monitors their swing, which is kept as low as possible by using eight glass spheres, of 25-kg net buoyancy each, in the top end of the mooring.

The thermistor strings are mounted in the center of the bottom lander, with a 1-m horizontal offset with respect to the central vertical axis of the upward-looking ADCP. This ADCP does ''hear'' the thermistor string, and especially the NFTS datalogger, but usually for brief periods of time only, and in a limited number of bins (Fig. 3). This occasional occurrence of erroneous data comes from the varying amounts of scattering material in the water and from the swinging of the string due to (tidal) current variations. Ensonification of the thermistor string is most recognizable in back-scattered ''echo intensity'' data. It also spoils current data, although to a lesser extent, because we programmed the ADCP by only storing data when ''all four beams provide good data,'' thereby filtering out some of the bad data. With some effort, and using echo intensity for tracing, current data can be corrected, when contaminated.

These observations are contrary to conclusions by Schott (1988), who described no substantial acoustic contamination from an Aanderaa thermistor string mounted directly in one of the beams of a 150-kHz ADCP. Perhaps his findings are biased as his observations are obtained in a lake, possibly carrying a high suspended material load. It is noted that our ADCPs

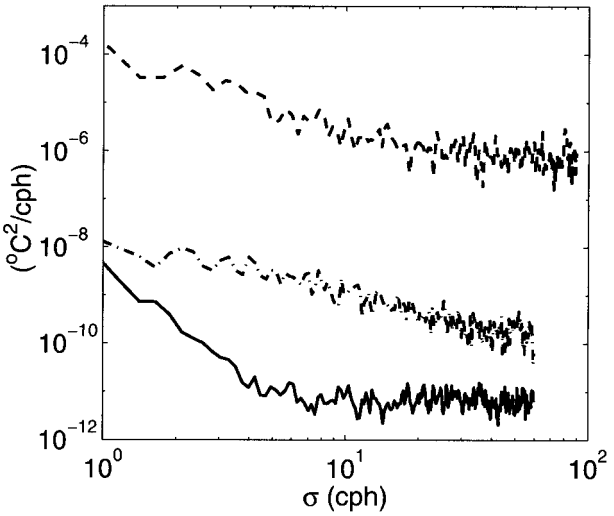

FIG. 4. High-frequency end of amplitude²-frequency (σ, in cycles per hour, cph) spectra of the temperature signal from one of the NFTS sensors to show noise characteristics under different conditions. The solid line indicates data from the laboratory test, revealing that instrumental noise is about five decades lower than the ''noise'' level of the signal measured in a tidal inlet (dashed line). During certain periods of time when the NFTS was properly moored in the northern North Sea, noise levels (dashed–dotted line) approach the laboratory test data. The tidal inlet data have been stored every 20 s, so that the Nyquist frequency is larger than for the other sets of data, stored every 30 s. The number of degrees of freedom (ν) indicating smoothing is about $\nu \approx 12$.

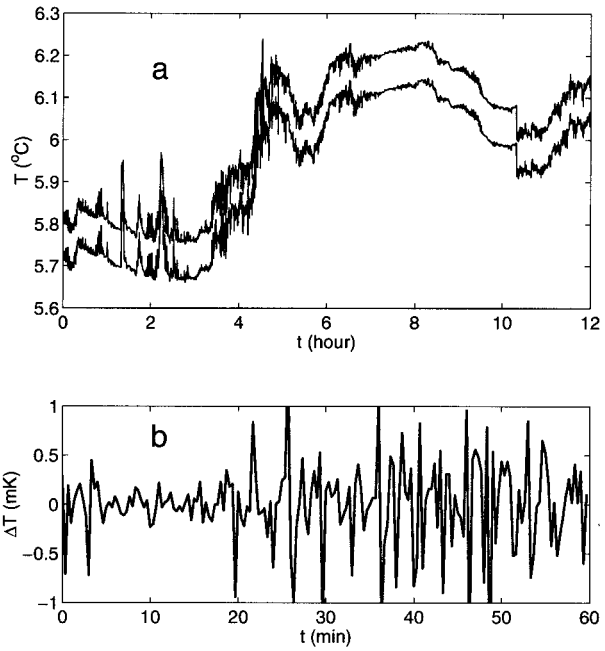

FIG. 5. (a) A portion of NFTS data from a tidal inlet. Tidal variation with time is visible, with some difficulty, in the temperature signal from two, arbitrarily chosen, sensors, which are offset by 0.09°C for clarity. Note the small variations with time and sudden ramps, simultaneously occurring in both sensors. (b) An example of 1 h of high-frequency (6 cph cutoff) temperature *difference* data between the two sensors in (a). The standard deviation of this signal is $\leq$0.4 mK. For the entire record of 14 h the overall standard deviation is about 10 mK.

operate at higher frequencies than Schott's and, more importantly, that the main umbilical of the NFTS is about two times thicker than an Aanderaa string, in addition to 3-cm-diameter-thick sensor bodies (Fig. 1). However, the example shown in Fig. 3 is the worst we observed in several deployments, and such contamination was almost negligible in measurements made above the continental slope in the Bay of Biscay (GV).

3. First results

During one of the laboratory calibrations an instrument noise test was performed, which was repeated in the field. So far, deployments of the NFTS in conjunction with the bottom-lander mooring have been partially successful. During the first two deployments at 800-m depth above the continental slope in the Bay of Biscay, oscillator cross talk increased the noise levels of the sensors to about 20 mK. During the first deployment in the northern North Sea after the subsequent repair of the NFTS, the upward-looking 600-kHz ADCP failed to record data. Fortunately, this last field experiment provided detailed internal wave temperature observations.

a. Laboratory noise test

The main noise source of the electronics of the NFTS was revealed by keeping it in the superbly isolated calibration bath without any stirring for a period of 5 days, while storing data every 30 s. It turned that dominant noise in the temperature signal came from quantization. This can be inferred from the lower trace in Fig. 4. The rms value of the high-frequency portion of the signal amounts to 36 μK, while the quantization (resolution) varies between 30 and 50 μK, depending on the temperature. Note that not all of the temperature variations are just random noise in this isolated bath as the spectrum is not white at the lower frequencies, and a (weak) day–night rhythm was still discernible in the time series.

b. Field noise test

The high-frequency part of the spectrum of temperature data measured during a field test showed much higher noise levels of 10 mK (upper trace in Fig. 4). For this test, the NFTS has been moored, coiled up, in a tidal inlet, where tidal currents reach up to 1.2 m s^{-1}. The measurement lasted 14 h, and data were stored every 20 s. Weather was calm. The measured ''noise'' is likely due to mooring vibrations and natural variability. It is not randomly distributed, despite its apparently flat appearance in the (high) frequency domain. This noise is highly dependent on the phase of the tide (Fig. 5). During periods of low current speeds, it drops below the required 1-mK level (Fig. 5b).

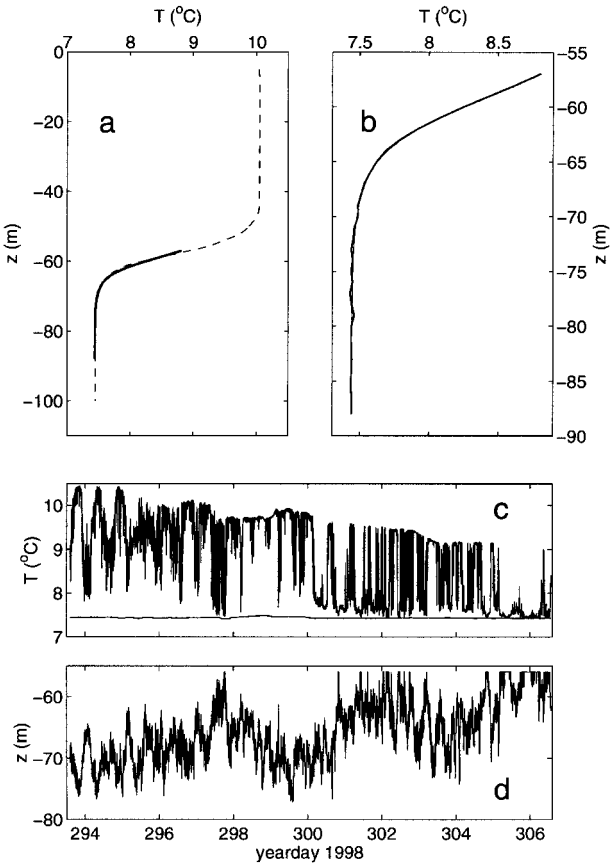

FIG. 6. Summary of northern North Sea data. (a) Average of 42 CTD profiles of temperature with depth (dashed line) obtained over the period of 14 days of mooring of the NFTS, of which the mean profile is given by the solid line. (b) Expansion of the depth coverage by the NFTS, showing the original mean data (thick, wiggling line) and the ''corrected'' mean as in (a) (thin line). (c) Temperature time series from upper- and lowermost NFTS thermistors. (d) Time series of the vertical displacements of the 7.5°C isotherm.

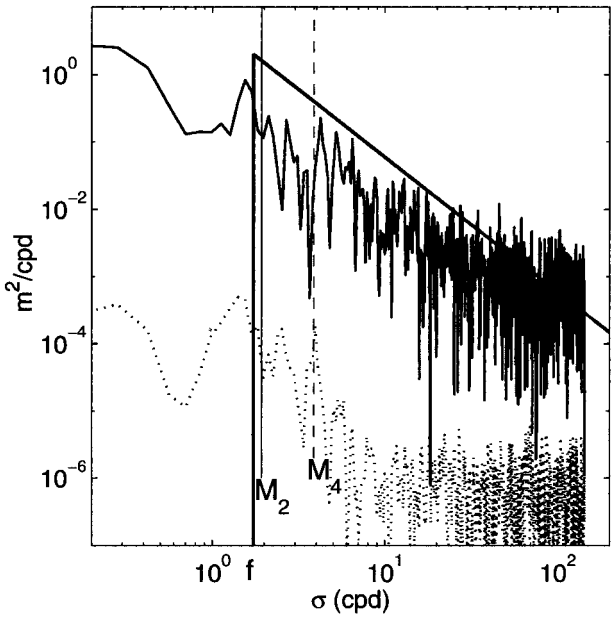

FIG. 7. Spectra (with frequency in cpd) of the first 7 days of displacements of the 7.5°C isotherm in Fig. 6d (solid line) and of the swaying of the top of the mooring as inferred from a tilt sensor (dotted line). For proper comparison, the isotherm data have been subsampled at once per 5 min, the sampling rate of the tilt meter, at the expense of aliasing signals near the buoyancy frequency. The number of degrees of freedom is low ($\nu \approx 4$) to resolve some of the inertial (f) and tidal harmonic (M_2 and M_4) frequencies. Schematically, the canonical internal wave spectrum is indicated by the solid triangular shape, indicating the σ^{-2} decrease with frequency.

c. Autumnal stratification in the northern North Sea

During Processes of Vertical Exchange in Shelf Seas (PROVESS), a project funded by the European Community in its Marine Science Programme EC-MAST3, the NFTS was moored in the northern North Sea. Around the mooring site, bottom topography is flat and featureless. The purpose of the project is to monitor the autumnal breakdown of the seasonal vertical stratification in density. The NFTS stored data every 30 s, for a period of 14 days (Fig. 6). Distributed over this period, 42 CTD casts were taken in the neighborhood of the mooring. Although the NFTS was located in the upper range of the 600-kHz ADCP (which did not function), the expected descent of the main thermocline did not occur during the mooring period, despite considerable wind forcing and consistently upward net heat flux, inducing surface layer cooling. As a result, the NFTS covered on average only the lower half of the thermocline (Fig. 6a), with a tide-dependent full coverage of this stratification in the beginning of the mooring period, and less of it later on (Figs. 6c,d). The NFTS was upright during the entire deployment period, swinging less than 5° according to the tilt meters.

After transfer of raw data to engineering units using the laboratory calibration results, the NFTS data showed systematic temperature differences (Fig. 6b), which are corrected using the mean CTD temperature data (Fig. 6a). The average correction amounts to 5 mK, which is somewhat larger than the expected inaccuracy following the laboratory calibrations. Overall, the performance of the NFTS was good, with very low noise levels measured occasionally (middle trace in Fig. 4). The data are only slightly spoiled by mooring motions, which in the vertical direction are considerably less, by two orders of magnitude, than the vertical displacements of levels of constant temperature (Fig. 7). These ''isotherm'' displacements, $\eta(T, t)$, have been obtained from the original temperature record $T(z, t)$ by the transfer $\delta\eta(T, t) = (\partial z/\partial T)\,\delta T(z, t)$.

The *T*–*S* relationship is reasonably tight, as can be inferred from the CTD data, with temperature contributing about 70% to density variations, and with salinity reenforcing stability induced by vertical temperature variations. A relationship between temperature (δT) and density variations ($\delta\rho$) is established as $\delta\rho = -(0.25 \pm 0.01)\delta T$. Using this relationship, the daily averaged

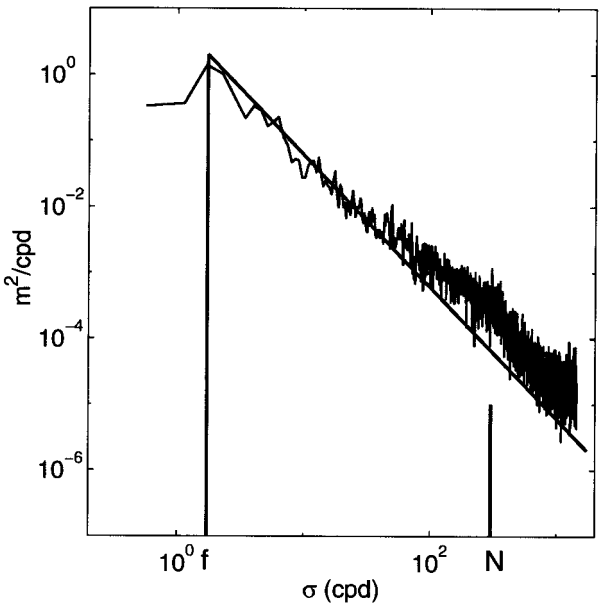

FIG. 8. Spectrum of vertical displacements of the 7.5°C isotherm as in Fig. 7 but slightly more smoothed ($\nu \sim 9$) and using the original sampling interval. Note the enhanced deviation from the canonical spectrum near the mean buoyancy frequency *N*, which is not a single harmonic frequency as depicted here, but its energy is smeared over about half a decade. This enhancement resembles theoretically predicted internal wave spectra at the buoyant frequency (Munk 1980).

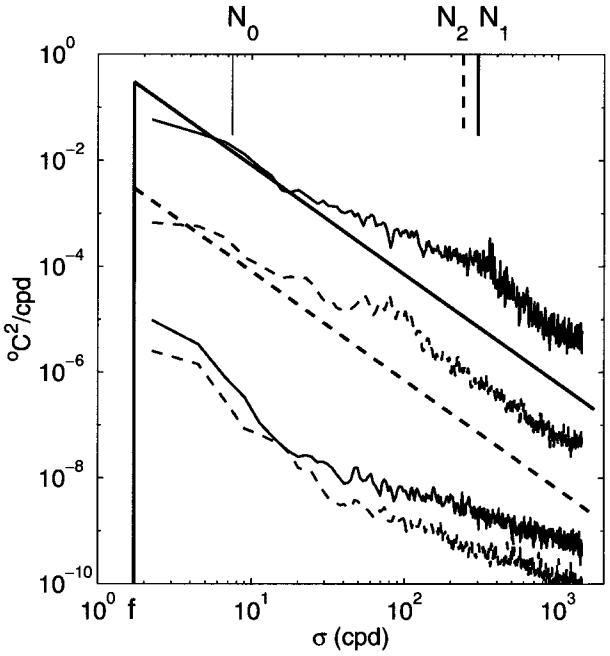

FIG. 9. Smoothed ($\nu \approx 15$) spectra of temperature autocovariance from data of the upper- and lowermost thermistors of the NFTS. The spectra have been computed for the first 7 days of data (solid lines), when the mean buoyancy frequency $N_1 \approx 300$ cpd (buoyancy period $T_{N1} \approx 300$ s), and for the last 7 days of data (dashed lines), when the mean buoyancy frequency $N_2 \approx 240$ cpd (buoyancy period $T_{N2} \approx 360$ s). Here, $N_0 \approx 7.5$ cpd is an estimate for the buoyancy frequency in the bottom boundary layer. The dashed line spectrum for the uppermost thermistor is lowered by two decades for clarity, together with its corresponding pictogram of the canonical spectrum.

(''mean'') buoyancy frequency varies between 200 and 800 cycles per day (cpd) within the main thermocline. As a result, the buoyancy period T_N, which is indicative of the shortest internal wave period, varies between $T_N = 100$ and 400 s. The NFTS sampled at a sufficiently high rate to resolve these buoyancy periods. To show its performance, we will focus on these short internal waves.

In general, amplitude^2-spectra of NFTS data correspond to the canonical internal wave spectrum (Figs. 8, 9). However, an enhanced deviation from the canonical spectrum is found between $0.2N < \sigma < N$, before rolling off. This can be seen in vertical displacement (potential energy) spectra (Fig. 8) and temperature variance spectra (Fig. 9). This enhancement, observed for the first time in the North Sea, and its extent in the frequency domain resemble a theoretical interpretation of free internal wave packets near the buoyant turning point (Munk 1980). Based on ocean observations (Cairns 1975) one decade lower infrequency than observed here, Munk predicted an amplification factor of $I(\sigma) \approx 2$ for displacement spectra near *N*, which he found relatively small because of the (power of 2) suppression of higher vertical modes. Figure 8 inhibits a precise determination of such an amplification factor, which we roughly estimate to be $1.5 < I(\sigma) < 5$. We attribute this imprecise estimate partially to smearing of energy near *N*, or to difficulties in defining *N*.

A (weak) variation in mean *N* seems to result in a shift of the enhanced values with frequency (Fig. 9). Puzzling are the smaller variations with frequency for *N*, with respect to the shifts for the enhancement peak. The weak variations for N correspond to the weak enhancement of the internal wave spectrum away from its boundaries ($f \ll \sigma \ll N$), assuming the canonical *N* scaling. However, the above observations require further investigation in which *N* is determined over shorter spans of time. It may be clear that these NFTS data are the adequate means for studies on enhanced high-frequency internal wave spectra over a flat bottom. They certainly are useful for studies on enhanced internal wave energy above sloping bottoms (e.g., Eriksen 1998).

Some of the variability and (ir)regularity of these high-frequency internal waves and the resolution thereof by the NFTS may be inferred from the time domain (Figs. 10–12). In Fig. 10, two different examples of tidal dominance are given. In one case, it is associated with a relatively weak main thermocline with a considerable amount of irregular high-frequency internal waves (Fig. 10a). In the second example, the main thermocline has considerably sharpened, supporting large and regular high-frequency internal waves (Fig. 10b). Sometimes, details show regular, almost linear, internal waves,

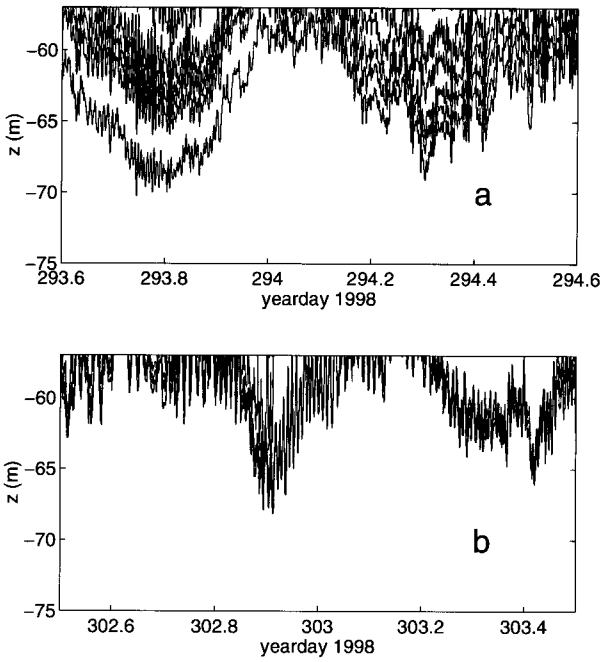

FIG. 10. Two different days of isotherm displacements. Isotherms are drawn every 0.5°C between 7.5° and 10.0°C.

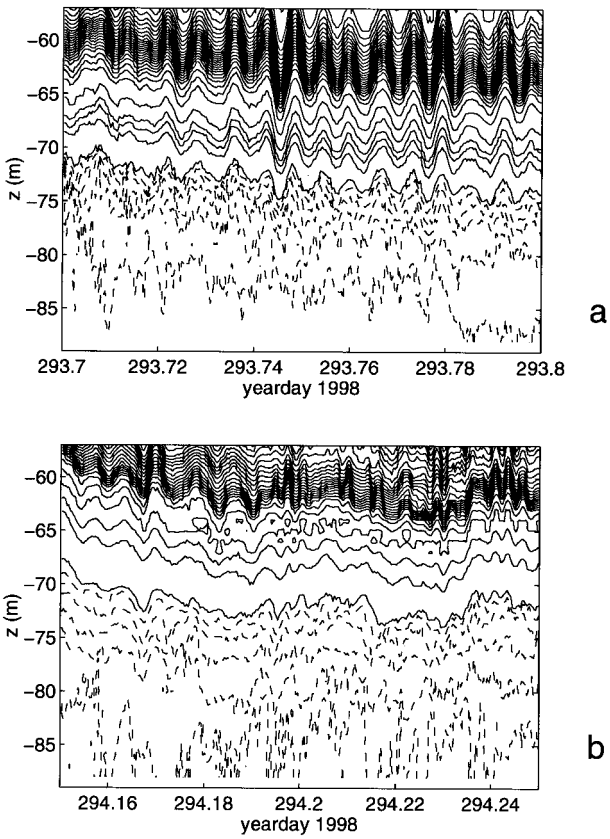

FIG. 11. Two examples of 0.1 days of isotherm displacements from the period in Fig. 10a. Isotherms are drawn every 0.1°C between 7.5° and 10.4°C (solid lines), and every 0.01°C between 7.41° and 7.49°C (dashed lines).

which are dominated by almost monochromatic waves having periods of 450 s, or 1.5 T_N (Fig. 11a). At other times, dominant high-frequency internal waves have periods close to T_N and show evidence of breaking. This can be inferred from the closed contours near 65-m depth between days 294.18 and 294.24 in Fig. 11b, which indicate static instabilities, assuming the *T–S* relationship is tight at these scales. These temperature inversions occur most often just below the main thermocline (note that we did not resolve the upper part properly), and occur for about an hour during the downward phase of the tide. They show anomalies down to −0.05°C, with little vertical extent (measured by one sensor only). Weaker anomalies of typically −0.0003°C extend over vertical scales up to 5 m (Fig. 12).

These temperature instabilities are observed when large high-frequency internal waves are present. These waves have typical periods of $2T_N$, but sometimes split (strain) so that virtually well mixed waters are separated by stronger vertical temperature gradients supporting internal waves above and below. Note that in this figure, the contouring in the lower part of the water column is at 1 mK. At these depths, regular waves and occasional breaking are alternated with irregular, but mostly stable, motions (from day 302.97 onward). The occurrence and variability of mixing events are our current subject of further investigation, but we may conclude that the capability of the NFTS is equal to highly sophisticated instrumentation like ''Bertha'' (Thorpe et al. 1990).

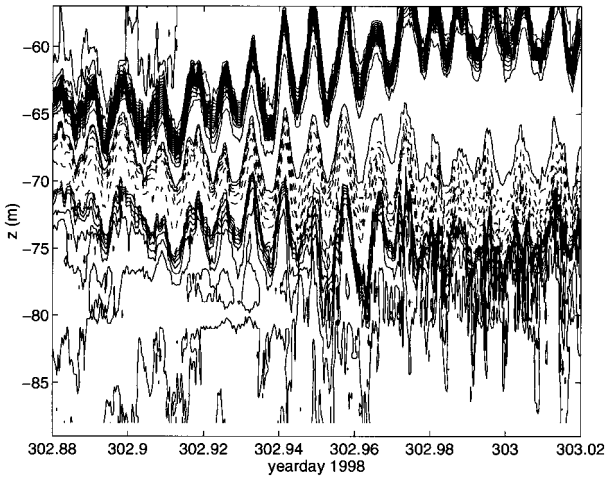

FIG. 12. Example of 0.14 days of isotherm displacements from the period in Fig. 10b. Isotherms are drawn every 0.1°C between 7.5° and 10.4°C (solid lines), every 0.01°C between 7.44° and 7.49°C (dashed lines), and every 0.001°C between 7.431° and 7.439°C (lower set of solid lines).

4. Summary and future development

We have presented some data from a newly built thermistor string, which is capable of measuring temperature variations at sea at an estimated accuracy of better than 0.5 mK. Calibrations are problematic and cannot be done better than within 3-mK accuracy. The thermistors have an impulse response time of approximately 0.25 s. The instrument is currently configured to address 32 sensors but is capable of addressing a maximum of 128 sensors.

The instrumentation has proven to be very robust and only one sensor has been broken so far, after several deployments at sea and corresponding rough treatments. Observations have shown that the noise level is dictated by quantization. The response time and accuracy, in combination with its wide range and endurance, allow the instrument to be used in any sea down to depths of 6000 m and prove it especially adequate for studies on internal waves up to the highest frequencies, including nonlinearities like internal bores.

Plans are made to improve the thermistor string, so that it will be more adapted for different environments. The sensor setup will become more intelligent, so that the user is able to choose between high accuracy at the expense of fast sampling, or fast sampling at the expense of high accuracy. We intend to develop synchronous sampling of all sensors, so that the fastest sampling rate will become about 0.1 s for the entire string. This initiative is motivated by the fact that high-frequency internal waves have not yet been observed using nearly instantaneous (or ''frozen field'') temperature profiles in strongly stratified environments, where the buoyancy period is O(min). Standard thermistor strings sample too slow (to our taste), and CTD profiles suffer from a lowering speed of typically 1 m s^{-1}. On the other hand, we aim to reduce self-heating to about 30 μK, and quantization to about 5–10 μK. The programming of the thermistor string will be more customized, for example to allow ''burst'' sampling to study fronts at the microstructure level. The cable harnass and interconnections will be miniaturized, and the number of sensors in the string will be increased to 128.

Acknowledgments. We thank the crew of the R/V *Pelagia* for deploying the ''mixBB'' bottom lander, which was built by Eduard Bos and Lorentz Boom. Jos Thieme and Sven Ober calibrated the NFTS in the laboratory. Theo Hillebrand took care of the test in the tidal inlet. Bert Aggenbach took the photos in Fig. 1 and Johannes Gemmrich created Fig. 2. We acknowledge advice by David Mills. The construction of the NFTS started during the Integrated North Sea Project, when HvH was supported by a grant from the Netherlands Organisation for the Advancement of Scientific Research, NWO. The field data presented in this paper have been collected within Processes of Vertical Exchange in Shelf Seas, a MAST3 project funded in part by the Commission of the European Communities Directorate General for Science and Education, Research and Development under Contract MAS3-CT97-0159.

REFERENCES

Armi, L., 1978: Some evidence for boundary mixing in the deep ocean. *J. Geophys. Res.,* **83,** 1971–1979.

Cairns, J. L., 1975: Internal wave measurements from a mid-water float. *J. Geophys. Res.,* **80,** 299–306.

Eriksen, C. C., 1985: Implications of ocean bottom reflection for internal wave spectra and mixing. *J. Phys. Oceanogr.,* **15,** 1145–1156.

——, 1998: Internal wave reflection and mixing at Fieberling Guyot. *J. Geophys. Res.,* **103,** 2977–2994.

Garrett, C. J. R., and W. H. Munk, 1979: Internal waves in the ocean. *Annu. Rev. Fluid Mech.,* **11,** 339–369.

Gilbert, D., 1993: A search for evidence of critical internal wave reflection on the continental rise off Nova Scotia. *Atmos.–Ocean,* **31,** 99–122.

Mihaly, S. F., R. E. Thomson, and A. B. Rabinovich, 1998: Evidence for nonlinear interaction between internal waves of inertial and semidiurnal frequency. *Geophys. Res. Lett.,* **25,** 1205–1208.

Munk, W. H., 1980: Internal wave spectra at the buoyant and inertial frequencies. *J. Phys. Oceanogr.,* **10,** 1718–1728.

——, 1981: Internal waves and small-scale processes. *Evolution of Physical Oceanography,* B. A. Warren and C. Wunsch, Eds., MIT Press, 264–291.

Pinkel, R., J. Sherman, J. Smith, and S. Anderson, 1991: Strain: Observations of the vertical gradient of isopycnal vertical displacement. *J. Phys. Oceanogr.,* **21,** 527–540.

Schott, F., 1988: Effects of a thermistor string mounted between the acoustic beams of an acoustic Doppler current profiler. *J. Atmos. Oceanic Technol.,* **5,** 154–159.

Thorpe, S. A., 1987: Current and temperature variability on the continental slope. *Philos. Trans. Roy. Soc. London,* **323A,** 471–517.

——, P. Hall, and M. White, 1990: The variability of mixing at the continental slope. *Philos. Trans. Roy. Soc. London,* **331A,** 183–194.

van Haren, H., N. Oakey, and C. Garrett, 1994: Measurements of internal wave band eddy fluxes above a sloping bottom. *J. Mar. Res.,* **52,** 909–946.

——, L. Maas, J. T. F. Zimmerman, H. Ridderinkhof, and H. Malschaert, 1999: Strong inertial currents and marginal internal wave stability in the central North Sea. *Geophys. Res. Lett.,* **26,** 2993–2996.